

Article

# Assessing Corrosion Fatigue Characteristics of Dissimilar Material Weld between Alloy617 and 12Cr Steel Using Buttering Welding Technique

Jeong Ho Hwang <sup>1</sup>, Ju Hwa Lee <sup>1</sup>, Hafiz Waqar Ahmad <sup>1</sup> , Seung Woo Ha <sup>2</sup>, Dong Ho Bae <sup>3,\*</sup> and Henok Yilma Kebede <sup>1,\*</sup>

<sup>1</sup> Graduate School of Mechanical Engineering, Sungkyunkwan University, Suwon ASI KR KS002, Korea; reflika@skku.edu (J.H.H.); juhwa0207@skku.edu (J.H.L.); waqar543@skku.edu (H.W.A.)

<sup>2</sup> Korea Leading Engineering System, Yuseong-gu, Daejeon ASI KR KS015, Korea; swha@kles.co.kr

<sup>3</sup> School of Mechanical Engineering, Sungkyunkwan University, Suwon ASI KR KS002, Korea

\* Correspondence: bae@yurim.skku.ac.kr (D.H.B.); henok@skku.edu (H.Y.K.); Tel.: +82-31-290-7443 (D.H.B.); +82-31-290-7479 (H.Y.K.)

Received: 4 September 2018; Accepted: 12 October 2018; Published: 15 October 2018



**Abstract:** In this study, dissimilar material welding between Alloy617 and 12Cr steel was performed using the buttering welding technique on the 12Cr steel side in order to increase the weldability. After multi-pass welding, post weld heat treatment (PWHT) was performed in order to reduce the welding residual stresses, and metallurgical microstructures were observed on dissimilar material weld. Additionally, the corrosion fatigue crack growth characteristics of dissimilar material weld was assessed according to Fracture Mechanics. Based on the results, the fatigue and corrosion fatigue strength of dissimilar material weld between Alloy617 and 12Cr steel did not show a big difference prior to and after post weld heat treatment. Fatigue and corrosion fatigue crack growth of dissimilar material weld were slightly faster than those of similar material weld of Alloy617. However, the characteristics of fatigue and corrosion fatigue crack growth did not show a big difference prior to and after PWHT.

**Keywords:** dissimilar material welding; mechanical property; corrosion fatigue; crack growth rate; post weld heat treatment

## 1. Introduction

Presently, the development of green energy and the reduction of environmental pollutants are urgent concerns in thermal power plants. Thus far, many researchers have attempted to develop technologies to solve these problems [1,2]. As a part of these efforts, some advanced countries have developed the A-USC (advanced ultra-super critical) thermal power plant, which operates steam turbines at high temperatures above 700 °C and at pressures above 250 bar. It is known that when the main steam temperature rises by 10 °C, the overall power generation efficiency is estimated to increase by more than 0.5% [3–6]. Developing suitable materials in these extreme operating conditions is difficult but necessary. Among the materials developed so far, the nickel-based alloys designated as Alloy617, Alloy625, and Alloy740 are good candidates as appropriate materials due to their excellent material properties such as heat resistance, corrosion resistance, and so on [7–9]. However, it is necessary firstly to guarantee the mechanical reliability of the weld for applying these Ni-based alloys to facilities of A-USC thermal power plant.

In the case of steam turbines, at the low pressure and temperature stage, corrosion and corrosion fatigue are considered to be the major damage mechanisms. Therefore, 12Cr steel is also an advisable applicant on this part due to its excellent corrosion resistance property. Furthermore, prime cost of

12Cr steel is much lower than that of Alloy617 [10]. So we suggest that in the high temperature and pressure stage, Alloy617 could be used, and a dissimilar material weld between Alloy617 and 12Cr steel could be used in the low pressure and temperature stage. The key technology for the application of 12Cr steel and Alloy617 to the low pressure and temperature stage is to develop and design a dissimilar material welding technology [11].

Therefore, in this study, dissimilar material welding between Alloy617 and 12Cr steel was performed using the buttering welding technique. Then, post weld heat treatment, observation of metallurgical microstructure, assessment of mechanical property, and corrosion fatigue crack growth characteristics were performed in order to secure the reliable fatigue design information on dissimilar material weld between Alloy617 and 12Cr steel.

## 2. Dissimilar Material Welding between Alloy617 and 12Cr Steel

### 2.1. Materials

Chemical compositions and mechanical properties are illustrated in Tables 1 and 2. The major compositions of Alloy617 are Ni, Cr, Co, and Mo. 12Cr steel has Cr and Fe as major compositions. In this study, Thyssen617 was used as filler metal for buttering welding and multi-pass dissimilar material welding. The major compositions of Thyssen617 are Ni, Cr, Co, and Mo, like those of Alloy617. The static tensile strength of dissimilar material weld prior to and after post weld heat treatment (PWHT) is compared in Table 2. Mechanical properties including yield strength, tensile strength, and elongation of dissimilar material weld are larger than 12Cr steel, but less than Alloy617.

**Table 1.** Chemical compositions of base metals (wt. %).

Base Metal	Ni	Cr	Co	Mo	Al	C	Mn	Fe	Si	S	Ti	Cu
Alloy617	Bal.	22	12.5	9	1.2	0.07	0.5	1.5	0.5	0.008	0.3	0.2
12Cr steel	0.43	11.62	-	0.04	-	0.13	0.58	Bal.	0.4	-	-	0.1
Thyssen617	Bal.	21.5	11.0	9.0	1.0	0.05	0.1	1.0	0.1	0.2	-	-

**Table 2.** Mechanical properties of Alloy617, 12Cr steel, and dissimilar material weld (reproduced from [12], with permission from World Scientific, 2018).

Material	Yield Strength (MPa)	Tensile Strength (MPa)	Elongation (%)	Reduction of Area (%)	Melting Point (°C)
Alloy617	322	734	62	56	1330
12Cr steel	551	758	18	50	1375
Dissimilar material weld prior to Post weld heat treatment	478	748	48	-	-
Dissimilar material weld after PWHT	496	735	42	-	-

### 2.2. The Procedure of Dissimilar Material Welding and Post Weld Heat Treatment

A narrow gap U-shaped groove was designed as illustrated in Figure 1. The 7-pass dissimilar material welding was performed using DCSP (direct current straight polarity) TIG (tungsten inert gas) welding technology. The welding processes including the electrode shape, arc length, welding wave mode (CW or pulse), welding heat input (voltage, current), and shield gas were controlled using a welding monitoring system (Monitech Co., Ltd., Busan, Korea). Welding conditions were determined through many repetitions of pre-welding tests. Prior to dissimilar material welding between Alloy617 and 12Cr steel, buttering welding was performed on the 12Cr steel side with Thyssen617 filler metal ( $\Phi = 1.6$ ) in order to increase the weldability between dissimilar materials. In the processes of multi-pass dissimilar material welding, when each pass was completed, the surface

condition of the weld bead was confirmed through the careful observation [13]. Table 3 shows the determined experimental conditions for buttering and multi-pass welding. The welding direction was made parallel to the rolling direction of base metal, as shown in Figure 2.

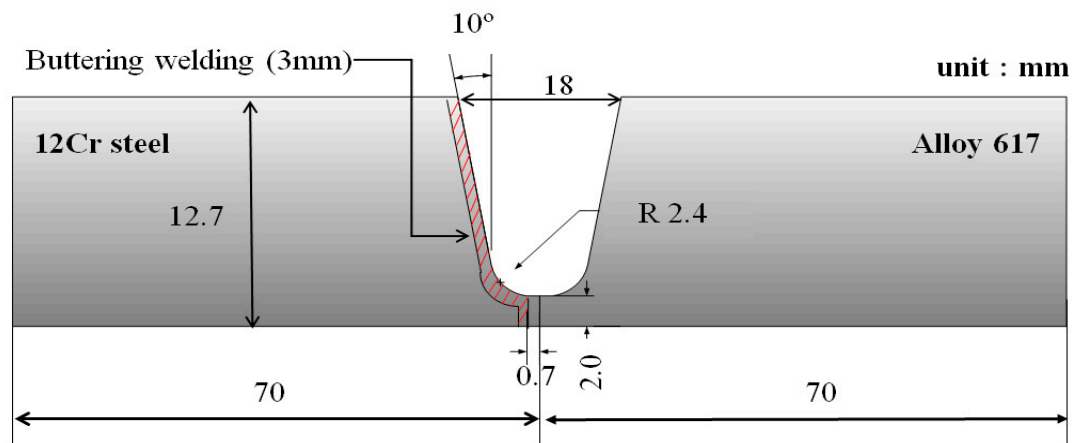


Figure 1. Design of narrow gap U-shaped groove.

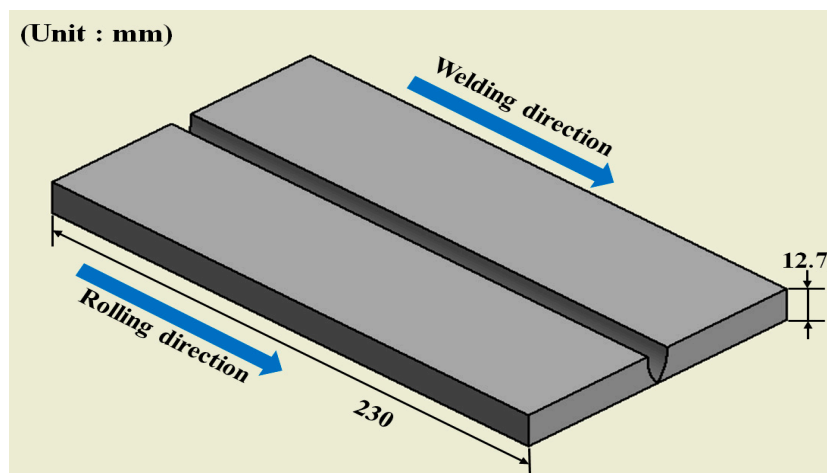


Figure 2. Welding direction.

Table 3. Dissimilar material welding conditions.

Pass	Shield Gas	Voltage (V)	Current (A)	Welding Speed (cm/min)	Heat Input (J/mm)
Butt.	Argon + 2.5% H <sub>2</sub>	120	10	10	0.9
1	Argon + 2.5% H <sub>2</sub>	120	10	10	0.9
2	Argon + 2.5% H <sub>2</sub>	150	13	10	1.17
3	Argon + 2.5% H <sub>2</sub>	180	16	10	1.44
4	Argon + 2.5% H <sub>2</sub>	180	16	10	1.44
5	Argon + 2.5% H <sub>2</sub>	180	16	10	1.44
6	Argon + 2.5% H <sub>2</sub>	180	16	10	1.44
7	Argon + 2.5% H <sub>2</sub>	180	16	10	1.44

Post weld heat treatment (PWHT) was performed in order to remove the welding residual stresses of dissimilar material weld. Figure 3 shows a schematic diagram of PWHT. PWHT was processed by heating time (heating rate: 220 °C/min)—holding time (4 h at 730 °C)—cooling time (furnace cooling), as shown in Figure 3 [14,15]. In the case of Alloy617 similar material welding, remarkable changes in mechanical properties were not found with PWHT [16].

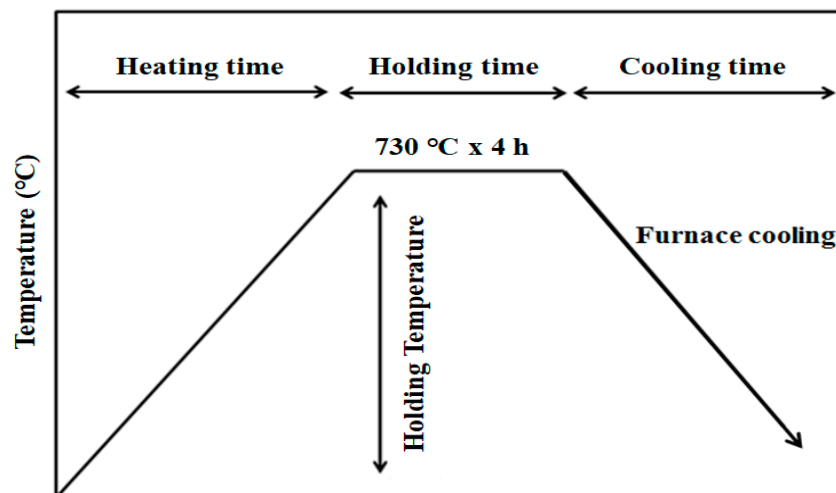


Figure 3. Schematic diagram of post weld heat treatment.

### 3. Metallurgical Microstructure and Chemical Composition Analysis of Dissimilar Material Weld

#### 3.1. Specimen and Procedure

In order to analyze metallurgical microstructures of the dissimilar material weld, optical microscope observation (JEOL Korea Ltd., Seoul, Korea) was conducted for the cross-section of the dissimilar material weld. The cross-section was divided into five regions as follows: (a) Alloy617 base metal, (b) Alloy617 heat affected zone (HAZ), (c) weld metal, (d) 12Cr steel HAZ, and (e) 12Cr steel base metal. These tests were performed in accordance with ASTM E407 [17]. The regions (a), (b), and (c) were etched with the etchant 88 (10 mL HNO<sub>3</sub> + 20 mL HCl + 30 mL distilled water) for 20 s, and the regions (d) and (e) were etched with etchant 91 (5 mL HNO<sub>3</sub> + 5 mL HCl + 1 g picric acid + 200 mL ethanol) for 10 s.

#### 3.2. Results and Discussion

Figure 4 shows the results of optical microscope observation prior to PWHT. The region (a) was basically dominant as the austenite grains [13,18]. The austenite grains were also observed at the region (b), however, the distribution of the grain size was irregular. The HAZ was heated to a high temperature by the heat transfer from the welding heat input. Therefore, since the grains were grown with heat, the grain sizes at the HAZ were very complicated according to a temperature gradient from the molten pool. In the region (c) of the weld metal, the dendrite grains were observed and grain sizes were much larger than those of the other regions. In the region (d), the martensite grains were observed, but the grains were deformed due to solid phase transformation by the welding heat input. Additionally, in region (e), the tempered martensite grains were observed. Figure 5 shows the optical observation after PWHT. There are few changes in (a), (b), and (c) regions. At the 12Cr steel HAZ, lath martensite grains were deformed by repetitive welding heat input. The changes due to PWHT were slight, except for in 12Cr steel HAZ. This is because, as is well known, Alloy617 is hardly affected by heat and has good heat-resistance. Whereas, in region (d), the shape of the grain was unchanged, but the grain size was larger than prior to PWHT. This is due to the fact that the post weld heat treatment had a tempering effect on this part.

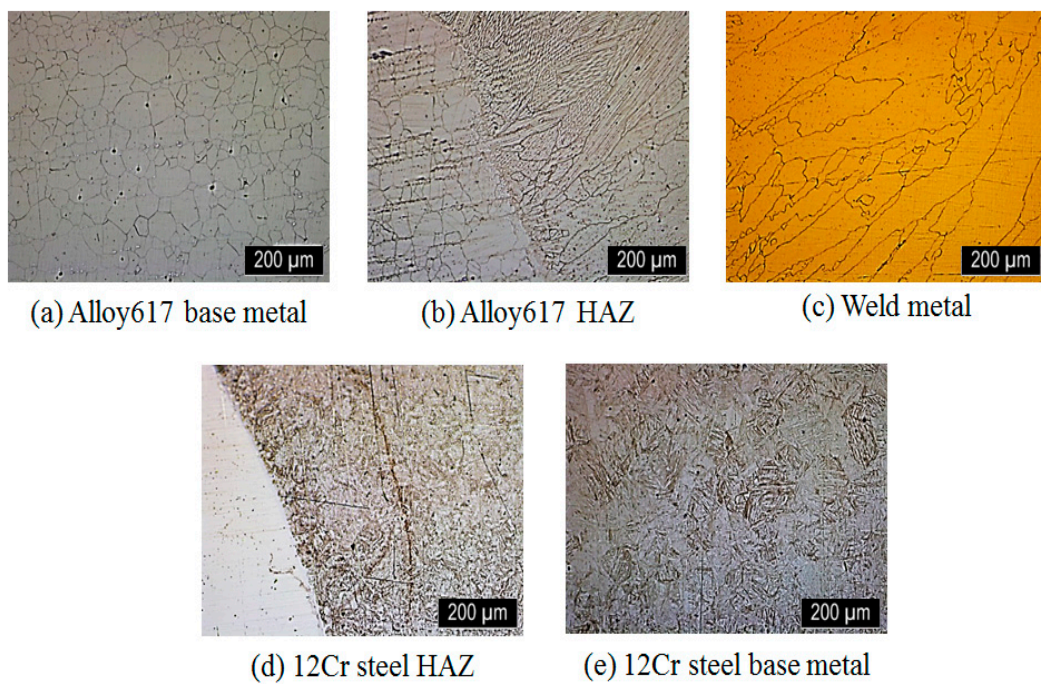


**Figure 4.** Optical microscope results prior to PWHT; (a) Alloy 617 base metal, (b) Alloy 617 heat affected zone, (c) Weld metal, (d) 12Cr steel HAZ, and (e) 12Cr steel base metal.

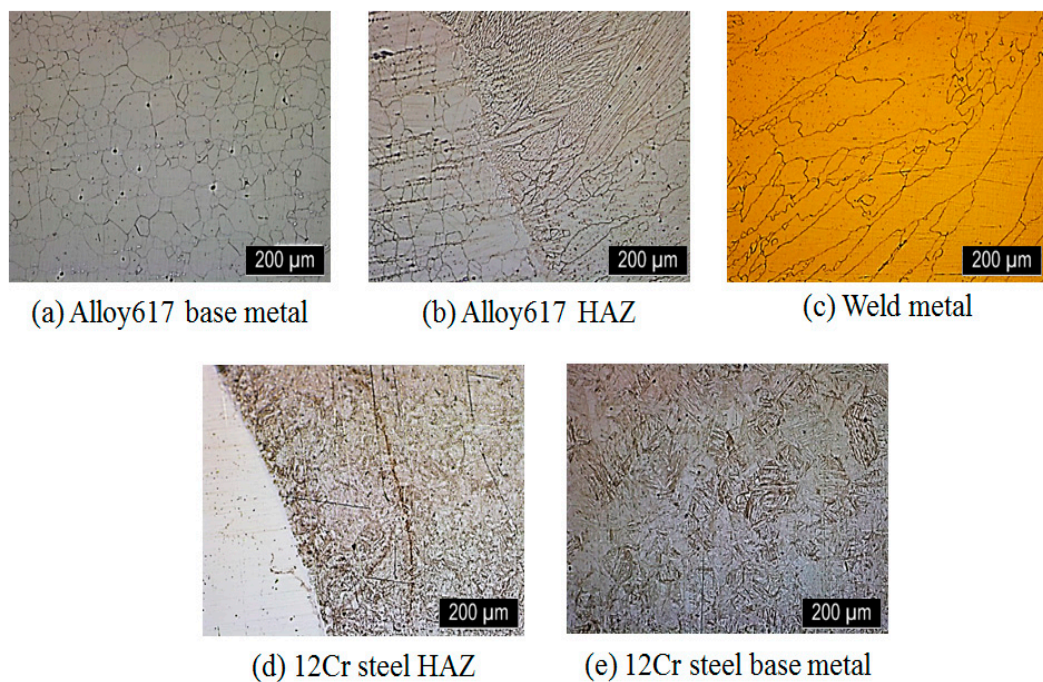


**Figure 5.** Optical microscope results after PWHT; (a) Alloy 617 base metal, (b) Alloy 617 HAZ, (c) Weld metal, (d) 12Cr steel HAZ, and (e) 12Cr steel base metal.

### 3.3. Chemical Composition Analysis

The chemical compositions of the dissimilar material weld were analyzed using SEM (scanning electron microscopy, JEOL. Korea Ltd., Seoul, Korea). As illustrated in Table 4, the major compositions at the base metal, HAZ, weld metal of the Alloy617 side are Mo, Cr, Co, and Ni. The Ni composition decreased slightly from the Alloy617 base metal to the weld metal. The other major compositions of Mo, Cr, and Co did not show big differences after welding. This is due to the fact that the compositions

of Alloy617 and Thysses617 are very similar, as illustrated in Table 1. The major compositions at the HAZ and base metal of 12Cr steel side were determined to be Cr and Fe. However, at the buttering weld metal, Mo, Cr, Fe, and Co were analyzed. This is due to the fact that the compositions of Thyssen617 and 12Cr steel were diluted in the process of buttering welding. Table 5 illustrates the chemical compositions analysis results after PWHT. The major compositions at dissimilar material weld between Alloy617 and 12Cr steel after PWHT were not remarkably changed. However, the decrease of Cr from 12Cr HAZ and base metal shown is due to the sensitization effect generated in the process of PWHT [19].

**Table 4.** Chemical compositions analysis results prior to PWHT (wt. %).

Elements	Alloy617 Base Metal	Alloy617 HAZ	Weld Metal	Buttering Weld Metal	12Cr HAZ	12Cr Base Metal
Mo	10.98	9.77	10.88	8.71	1.36	-
Cr	22.03	20.25	20.31	21.59	11.80	11.84
Fe	-	2.29	3.00	13.13	85.56	86.93
Co	12.47	11.95	12.31	10.68	-	-
Ni	54.07	53.17	51.25	45.89	-	-

**Table 5.** Chemical compositions analysis results after PWHT (wt. %).

Elements	Alloy617 Base Metal	Alloy617 HAZ	Weld Metal	Buttering Weld Metal	12Cr HAZ	12Cr Base Metal
Mo	10.87	10.15	10.56	8.94	1.27	-
Cr	22.26	21.19	20.83	21.39	10.56	10.28
Fe	-	2.48	3.11	13.25	86.69	88.43
Co	12.43	11.84	12.46	10.71	-	-
Ni	54.03	53.08	51.86	45.53	-	-

#### 4. Assessing Fatigue Strength of the Dissimilar Material Welded Joint

##### 4.1. Specimen and Equipment

Figure 6 shows the configuration of tensile and fatigue test specimen. The test specimen includes the weld metal, HAZ, and base metals of dissimilar material welded joint between Alloy617 and 12Cr steel. All specimens were prepared in the perpendicular direction to the weld line and machined in accordance with the ASTM E8M standard [20]. The material testing system (Instron Korea, Seoul, Korea) was used for tensile and fatigue tests as shown in Figure 7.

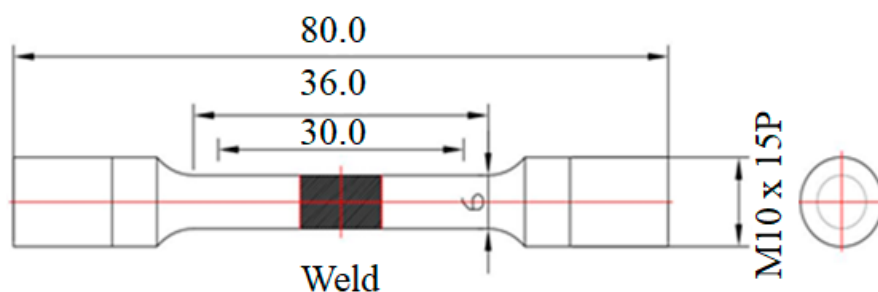


**Figure 6.** Specimen for mechanical property test.



**Figure 7.** Material testing system (Instron 8801, 10 tons).

#### 4.2. Test Conditions and Procedure

Table 6 illustrates fatigue test conditions in air prior to and after PWHT. The fatigue tests in air were carried out by applying the load decreasing method, and the fatigue tests started from  $\sigma_{\max} = 673.2$  MPa prior to PWHT and  $\sigma_{\max} = 661.5$  MPa after PWHT, which corresponds to 90% of the static tensile strength ( $(\sigma_u)_{\text{before}} = 748$  MPa and  $(\sigma_u)_{\text{after}} = 735$  MPa) prior to and after PWHT of the dissimilar material weld. The load ratio ( $R = P_{\min}/P_{\max}$ ) was 0.1, the frequency was 10 Hz, the loading type was sinusoidal, and the fatigue limit was determined by the load at which the fatigue test specimen did not fail up to  $10^6$  cycles. Corrosion fatigue tests were also carried out using the load decreasing method. Table 7 illustrates the corrosion fatigue test conditions under pH = 3.5, 3.5 wt. % NaCl solution. It is known that corrosion fatigue is to occur at the outlet conditions of steam turbines. These are the real operating conditions (1 atm, 70 °C) of the low pressure and temperature stage of steam turbine. The introduction of chemical cleansings and seawater creates this unique corrosive medium. Corrosion fatigue tests started from  $\sigma_{\max} = 294.12$  MPa, which corresponds to the 90% of the fatigue limit in air of dissimilar material weld (= 326.8 MPa). In corrosion fatigue tests, applied the load ratio ( $R$ ) and loading type were the same as those in air. However, the frequency applied was 1 Hz to make a corrosion reaction between the surface of specimen and corrosive solution.

**Table 6.** Conditions of fatigue test in air.

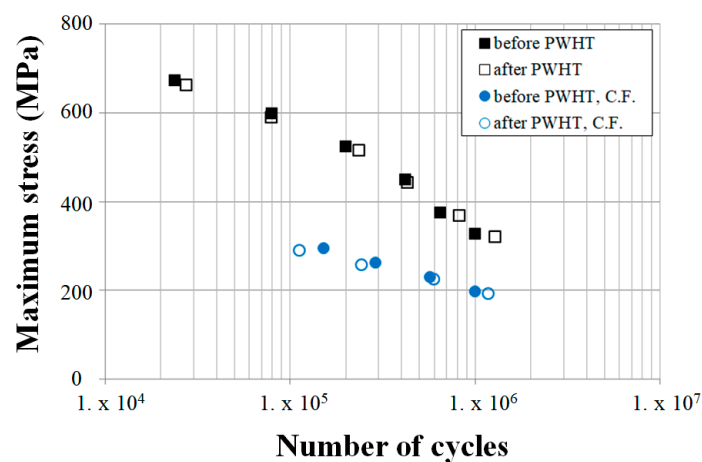
Load Ratio ( $R$ )	Frequency	Applied Load (MPa)	
		Prior to PWHT	After PWHT
0.1	10 Hz	$0.9\sigma_u = 673.2$	$0.9\sigma_u = 661.5$
		$0.8\sigma_u = 598.4$	$0.8\sigma_u = 588.0$
		$0.7\sigma_u = 523.6$	$0.7\sigma_u = 514.0$
		$0.6\sigma_u = 448.8$	$0.6\sigma_u = 441.0$
		$0.5\sigma_u = 374.0$	$0.5\sigma_u = 367.5$
		$0.45\sigma_u = 326.8$	$0.45\sigma_u = 319.7$

**Table 7.** Conditions of corrosion fatigue test.

Load Ratio (R)	Frequency	Applied Load (MPa)	
		Prior to PWHT	After PWHT
0.1	1 Hz	$0.9\sigma_L = 294.12$	$0.9\sigma_L = 287.73$
		$0.8\sigma_L = 261.44$	$0.8\sigma_L = 255.76$
		$0.7\sigma_L = 228.76$	$0.7\sigma_L = 223.79$
		$0.6\sigma_L = 196.08$	$0.6\sigma_L = 191.82$
Environmental conditions	Temp.	70 °C	70 °C
	Solution	NaCl 3.5 wt. % pH = 3.5	NaCl 3.5 wt. % pH = 3.5

#### 4.3. Results and Discussion

The S-N curves of the dissimilar material welded joints between Alloy617 and 12Cr steel in air and in a corrosive environment prior to and after PWHT were compared in Figure 8. The plotted data indicates the mean values of the fatigue data obtained by the three time tests. Fatigue and corrosion fatigue test specimens failed at the HAZ of 12Cr steel. This is due to the fact that the material properties of two base metals. The chemical compositions of Alloy617 base metal, buttering weld and weld metal are similar but those of 12Cr steel are far different as shown in Table 1. And the magnitude of welding residual stresses of 12Cr steel HAZ was much higher than that of Alloy617 HAZ [12]. Furthermore, metallurgical changes generated in the process of buttering welding and multi-pass dissimilar material welding were different, as illustrated in Figures 4 and 5. Fatigue strength in air for prior to and after PWHT did not show a big difference. However, the fatigue limits prior to and after PWHT were assessed at 326.8 MPa and 319.7 MPa, which are approximately 45% of the static tensile strength of the dissimilar material weld prior to PWHT (748 MPa) and after PWHT (735 MPa). The corrosion fatigue strength of dissimilar material welded joints between Alloy617 and 12Cr steel was lower than those in air. These results are due to the fact that, apart from the differences of material properties of two base metals and the magnitude of welding residual stresses and metallurgical changes mentioned above, as is well known Alloy617 has excellent thermal properties but the 12Cr steel does not [7–9]. From the results, the corrosion fatigue limits prior to and after PWHT were assessed at 196.08 MPa and 191.82 MPa, which are 60% of the fatigue limits of dissimilar material weld prior to PWHT (326.8 MPa) and after PWHT (319.7 MPa).

**Figure 8.** Comparison of fatigue and corrosion fatigue strength between prior to and after PWHT.

## 5. Assessing Fatigue Crack Growth Characteristics of the Dissimilar Material Weld below the Fatigue Limit

### 5.1. Test Specimen and Procedure

The test specimen for assessing corrosion fatigue crack growth characteristics was designed and manufactured as CT (compact tension) type recommended in ASTM E647 as shown in Figure 9 [19]. The CT specimen includes the weld metal, the HAZs of the both sides, and the base metals. As illustrated in Section 4.3, since the fatigue specimen was mostly failed at the HAZ on the 12Cr steel side of dissimilar material weld, a notch for precrack of the specimen was machined at the HAZ on the 12Cr steel side by electric discharge machining technology. All specimens were precracked 3 mm before the test [21]. The test equipment used was a material testing system of Figure 7. The fatigue and corrosion fatigue tests were conducted under the conditions illustrated in Tables 8 and 9. The tests started from the low limits of the dissimilar material welded joint of Figure 8, respectively. In order to measure fatigue crack growth on real time, electric potential variation during fatigue crack growth was measured by the DCPD (direct current potential drop) method using the nano volt meter (Agilent Co. model 34420A, Daegu, Korea). Additionally, the crack length increase by fatigue crack growth was calculated using a correction curve which indicates the relationship between electric potential and crack length in air.

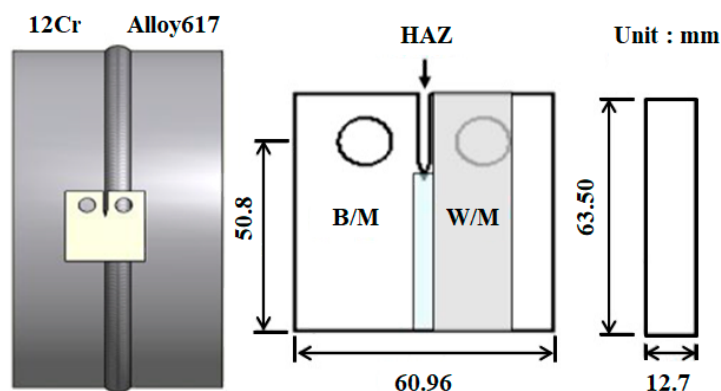


Figure 9. Corrosion fatigue test results comparison of prior to and after PWHT.

Table 8. Tests conditions for fatigue crack growth rate.

Conditions		Contents	
		Prior to PWHT	After PWHT
Loading condition	Maximum Load	12,334 kN	12,066 kN
Environmental condition	Temp.	Real temperature	R.T.
	Solution	In air	In air

Table 9. Test conditions for corrosion fatigue crack growth rate.

Conditions		Contents	
		Prior to PWHT	After PWHT
Loading condition	Maximum Load	7400 kN	7239 kN
Environmental condition	Temp.	70 °C	70 °C
	Solution	NaCl 3.5 wt. % pH = 3.5	NaCl 3.5 wt. % pH = 3.5

## 5.2. Results and Discussion

Figures 10 and 11 show the relationships between the crack growth rate ( $da/dN$ ) and the stress intensity factor range ( $\Delta K$ ) in air and in corrosion environment. Alloy617 similar welds' results [12] were used as reference data for comparison with dissimilar material weld. In Figure 10, crack growth rate at the HAZ of 12Cr steel prior to PWHT is slightly faster than after PWHT in the large  $\Delta K$  range. This is due to the removal of welding residual stresses by PWHT and metallurgical change (sensitization) by multi-pass welding and PWHT. In the case of Alloy617 similar weld, the crack growth rate after PWHT was faster than that prior to PWHT. This is due to the fact that Alloy617 was influenced by PWHT [13]. However, it does not show a big difference between similar and dissimilar material weld in air. Table 10 illustrates the  $C$  and  $m$  values of Paris' law. In Figure 11, the corrosion fatigue crack growth rates at the HAZ of 12Cr steel before PWHT is slightly faster than after PWHT in the large  $\Delta K$  range, like that in air. This is due to corrosion sensitivity from removing welding residual stresses and metallurgical change including sensitization by multi-pass welding and PWHT. In the case of an Alloy617 similar weld, the corrosion fatigue crack growth rates do not show any difference prior to and after PWHT. This is due to the fact that Ni-based Alloy617 has excellent heat and corrosion resistant characteristics. However, even though the corrosion fatigue crack growth rates do not show a big difference between similar and dissimilar material weld as shown in Figure 11, the corrosion fatigue crack growth rates both prior to and after PWHT are faster than those in air. The  $C$  and  $m$  values of Paris' law in corrosion fatigue are arranged in Table 10.

**Table 10.** Experimental estimation of  $C$  and  $m$  of Paris' law.

Conditions		$m$	$C$ (m/cycle)
In air	Prior to PWHT	4.97	$3.20 \times 10^{-12}$
	After PWHT	4.71	$7.00 \times 10^{-12}$
In corrosion	Prior to PWHT	6.51	$2.53 \times 10^{-14}$
	After PWHT	6.31	$3.88 \times 10^{-14}$

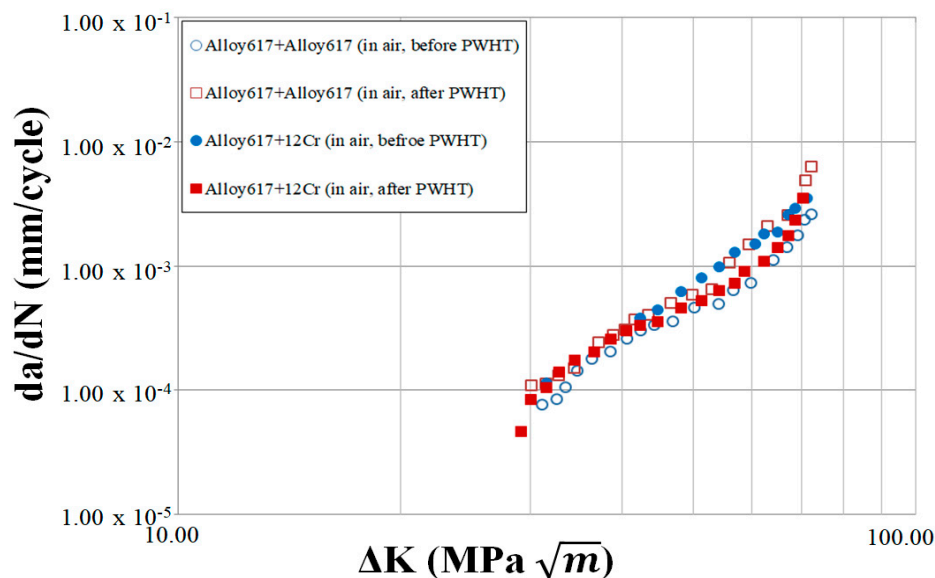


**Figure 10.** Relationship between  $da/dN$ – $\Delta K$  in air (reproduced from [12], with permission from World Scientific, 2018).

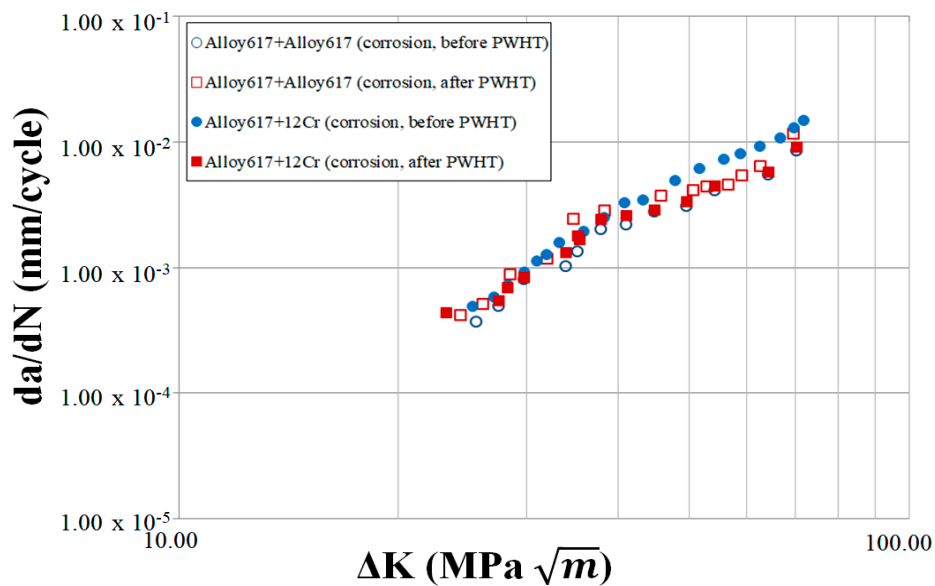


Figure 11. Relationship between  $da/dN$ – $\Delta K$  in corrosion environment.

## 6. Conclusions

This study aimed to secure the reliability of the dissimilar material welding between Alloy617 and 12Cr steel using the buttering welding technique, metallurgical microstructure analysis, and assessment of corrosion fatigue crack growth characteristics.

The summarized conclusions are as follows:

1. Dissimilar material welding technology between Alloy617 and 12Cr steel using the buttering welding technique on the 12Cr steel side has been proposed.
2. In the case of dissimilar material welding between Alloy617 and 12Cr steel, microstructures of base metal, HAZ, and weld metal of the Alloy617 side are not remarkably changed. However, metallurgical microstructures of the 12Cr steel side are influenced by the heat transfer from repeated welding heat input during the multi-pass welding process.
3. Low limits of fatigue strength and corrosion fatigue strength for dissimilar material welded joint were assessed by 326.8 MPa and 196.08 MPa prior to PWHT, and 319.7 MPa and 191.82 MPa after PWHT. Low fatigue and corrosion fatigue limits both prior to and after PWHT do not show a big difference, as about 45% of static tensile strength and 60% of the low fatigue limits of dissimilar material welded joint.
4. Crack growth rate at the HAZ of 12Cr steel prior to PWHT is slightly faster than after PWHT in the large  $\Delta K$  range. However, it does not show a big difference between similar and dissimilar material weld in air. Corrosion fatigue crack growth rates at the HAZ of 12Cr steel prior to PWHT is slightly faster than before PWHT in the large  $\Delta K$  range like that in air. However, even though the corrosion fatigue crack growth rates do not show a big difference between similar and dissimilar material weld, the corrosion fatigue crack growth rates of both prior to and after PWHT are faster than those in air.

**Author Contributions:** J.H.H. conceived and designed the experiments; J.H.H., J.H.L., H.W.A. and S.W.H. performed the experiments and analyzed the data under supervision of D.H.B. and H.Y.K.; J.H.H. wrote the paper.

**Funding:** This research received no external funding.

**Acknowledgments:** This work was supported by the Reliability Evaluation Laboratory of the Mechanical Engineering Department, Sungkyunkwan University, Suwon, Korea.

**Conflicts of Interest:** The authors declare no conflict of interest.

## References

1. Li, Y.W.; Chen, J. A novel nonlinear model of rotor bearing seal system and numerical analysis. *Mech. Mach. Theory* **2011**, *46*, 618–631. [[CrossRef](#)]
2. Nowak, G.; Rusin, A. Shape and operation optimization of supercritical steam turbine rotor. *Energy Convers. Manag.* **2013**, *74*, 416–425. [[CrossRef](#)]
3. Kosman, W.; Roskosz, A.; Nawrat, K. Thermal elongations in steam turbine with welded rotors made of advanced materials at supercritical steam parameters. *Appl. Therm. Eng.* **2009**, *29*, 3393–3396. [[CrossRef](#)]
4. Kosman, W. Thermal analysis of cooled supercritical steam turbine components. *Energy* **2010**, *29*, 1181–1187. [[CrossRef](#)]
5. Rusin, A.; Nowak, G.; Piecaha, W. Shrink connection modeling of steam turbine rotor. *Eng. Fail. Anal.* **2013**, *34*, 217–227. [[CrossRef](#)]
6. Sun, Y.J.; Liu, X.Q.; Hu, L.S.; Tang, X.Y. Online life estimation for steam turbine rotor. *J. Loss Prev. Process Ind.* **2013**, *26*, 272–279. [[CrossRef](#)]
7. El-Awadi, G.A.; Abdel-Samad, S.; Elshazly, E.S. Hot corrosion behavior of Ni based Inconel 617 and Inconel 738. *Appl. Surf. Sci.* **2016**, *378*, 224–230. [[CrossRef](#)]
8. Green, M.A. High Efficiency Silicon Solar Cells. In Proceedings of the Seventh EC Photovoltaic Solar Energy Conference, Sevilla, Spain, 27–31 October 1986; Springer: Dordrecht, The Netherlands, 1987.
9. Nandi, S.; Reddy, G.J.; Singh, K. Microstructural Changes in IN617 Superalloy during Creep at High Temperature. *Procedia Eng.* **2011**, *10*, 2645–2650. [[CrossRef](#)]
10. Masuyama, F. History of Power Plants and Progress in Heat Resistant Steel. *ISIJ Int.* **2001**, *41*, 612–625. [[CrossRef](#)]
11. Fukuda, M. Advanced USC technology development in Japan. *IJIS Int.* **2001**, *41*, 612–625.
12. Hwang, J.H.; Lee, J.H.; Bae, D.H. Welding residual stress effect of the fatigue strength at dissimilar material weld between Alloy617 and 12Cr steel. *Int. J. Mod. Phys. B* **2018**, *32*, 1–5. [[CrossRef](#)]
13. Park, Y.S.; Bae, D.H. Assessment of the crack growth characteristics at the low fatigue limit of a multi-pass welded Ni-based alloy 617. *J. Mech. Sci. Technol.* **2014**, *28*, 1251–1256. [[CrossRef](#)]
14. Tian, Z.L.; Coussement, C.; Witte, M.D.; Steen, M. Creep Behavior of 12Cr-Mo-V Steel Weldments. *Int. J. Press. Vessel. Pip.* **1991**, *46*, 339–349. [[CrossRef](#)]
15. Andren, H.O.; Cai, G.; Svensson, L.E. Microstructure of heat resistant chromium steel weld metals. *Appl. Surf. Sci.* **1995**, *87*, 200–206. [[CrossRef](#)]
16. Park, Y.S.; Choi, J.J.; Bae, D.H. Fracture Mechanical Assessment of the Corrosion Fatigue Characteristics at the Low Fatigue Limit of a Multi-pass Welded Ni-Based Alloy 617. *Procedia Mater. Sci.* **2014**, *3*, 1530–1535. [[CrossRef](#)]
17. ASTM E407-07. *Standard Practice for Micro-Etching Metals and Alloys*; ASTM: West Conshohocken, PA, USA, 2015.
18. Ahmad, H.W.; Hwang, J.H.; Lee, J.H.; Bae, D.H. An Assessment of the Mechanical Properties and Microstructural Analysis of Dissimilar Material Welded Joint between Alloy 617 and 12Cr Steel. *Metals* **2016**, *6*. [[CrossRef](#)]
19. Poulson, B. The sensitization of ferritic steels containing less than 12% Cr. *Corros. Sci.* **1978**, *18*, 371–395. [[CrossRef](#)]
20. Standard Test Method for Tension Testing of Metallic Materials. Available online: <https://www.astm.org/Standards/E8.htm> (accessed on 17 July 2018).
21. ASTM International. *Standard Test Method for Measurement of Fatigue Crack Growth Rates*; ASTM International: West Conshohocken, PA, USA, 2011.

